J. Fluid Mech. (1981), *vol.* 105, *pp.* 397–425
Printed in Great Britain

Buffeting forces on rigid circular cylinders in cross flows

By RONALD M. C. SO AND SUDHIR D. SAVKAR

Corporate Research and Development Center, General Electric Company, Schenectady, New York 12301

(Received 29 October 1979 and in revised form 8 July 1980)

Experimentally measured steady and unsteady forces induced by a cross flow over a smooth circular cylinder are reported in this paper. The measurements were made in the 0·305 m research water tunnel of the Pennsylvania State University. The parameters examined include the Reynolds number, which was varied over a range of 2×10^4 to 2×10^6, free-stream turbulent intensity, integral length scale-to-diameter ratio and active span-to-diameter ratio; however, this paper includes only some of these results.

Among the results reported are the complete mean drag data on all the cylinders tested and some fluctuating force data chosen to illustrate the effects of Reynolds number and active span-to-diameter ratio on the measured forces in uniform and turbulent cross flows. From these results, it can be concluded that the unsteady forces bear a functional relation to Reynolds number in the range tested which is very similar to the well-documented behaviour of the mean drag. Thus the effect of free-stream turbulence on both the steady drag forces and the unsteady forces is to shift the transitional region to a lower Reynolds number. Decreasing the active span-to-diameter ratio increases the buffeting lift coefficient at the same Reynolds number. Finally, it is observed that the Strouhal lift signal at transitional Reynolds numbers is no longer quasi-periodic but rather resembles a narrow-band random signal.

1. Introduction

It has long been recognized that turbulence in the free stream can induce early transition of the flow around a circular cylinder and hence reduce the steady drag coefficient of the cylinder in the range of transitional Reynolds numbers (Goldstein 1965). In spite of the extensive work carried out by numerous researchers (such as Relf & Simmons 1924; Fung 1960; Roshko 1961; Bishop & Hassan 1964; Jones, Cincotta & Walker 1968; Richter & Naudascher 1976; to name a few) on the fluctuating responses of rigid cylinders in uniform cross flows, the related phenomenon of free-stream turbulence effects on the induced unsteady forces has received scant attention to date. However, the problem is of growing concern to engineers who work in the area of fluid–structure interactions. This is especially true in the design of nuclear reactor components, large stacks and other like structures.

The paucity of data in this area can be seen by examining figure 1 where some of the more important work on Strouhal excitation (due to uniform cross flows) and buffeting forces (due to turbulent cross flows) on rigid cylinders as a function of Reynolds number, *Re*, has been summarized. In figure 1, open rectangles represent work carried out on the Strouhal phenomenon, while the hatched rectangles represent work carried

0022-1120/81/4686-3780 $02.00

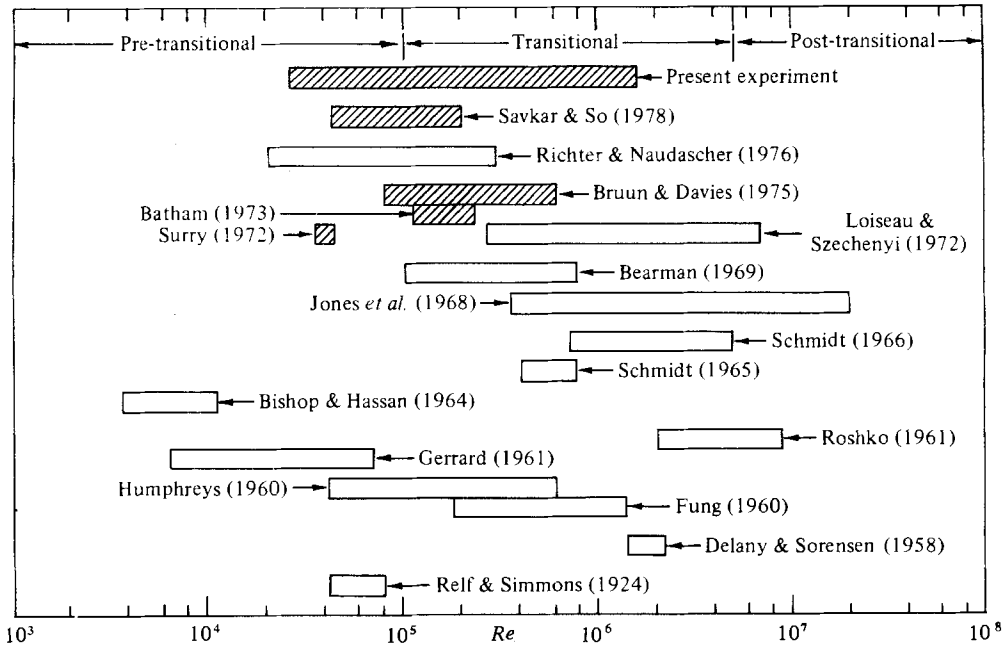

FIGURE 1. Summary of work on fluctuating forces on rigid circular cylinders in cross flows.

out on both the Strouhal and buffeting phenomena. Most of the work performed in the past was to investigate the Strouhal excitation on single cylinders, and the unsteady lift was measured as a function of Reynolds number which varied from 4×10^3 to 2×10^7. Therefore, our knowledge of the Strouhal phenomenon is substantial. The buffeting phenomenon has not been as extensively investigated. With the exception of Savkar & So (1978), none of the prior studies appears to have measured the unsteady buffeting forces induced on circular cylinders directly. The bulk of the observations were restricted to the measurement of unsteady pressures.

Surry (1972) investigated the influence of free-stream turbulence on the unsteady pressure distribution around a cylinder within the subcritical range of Reynolds numbers. The intensity of turbulence at the model location was in excess of 10 % and the integral length scales were varied from 0·36 to 4·4 diameters. However, the intensity was not held fixed over the range of scales tested. In the subcritical flow regime, Surry found that even such intense turbulence failed to disrupt the distinct vortex shedding. Turbulence did appear to broaden the Strouhal peak and significantly increase the response in the low frequency range below the Strouhal frequency. Information about the fluctuating lift and drag was deduced from correlations measured in one of the four cases tested. These measurements serve to illustrate the complexity and difficulty of inferring the unsteady force from distributed unsteady pressure measurements.

Batham (1973) conducted measurements similar to Surry's at the critical Reynolds number on both a smooth cylinder and a cylinder artificially roughened by sand. Free-stream turbulence of high intensity (in excess of 10 %) and integral scale roughly half the diameter was found to suppress coherent vortex shedding from a smooth cylinder. On the other hand, the turbulence gave rise to an increase in the level of vortex shedding energy for the rough cylinder. From an interpretation of the mean

pressure distribution, Batham suggested that the rough cylinder should simulate the supercritical behaviour of smooth cylinders, say, operating at Reynolds numbers in the vicinity of 10^7.

Bruun & Davies (1975) covered roughly the same range of parameters as Batham but restricted their study primarily to a smooth cylinder. As observed by Batham (1973), Bruun & Davies also reported a substantial reduction in the spanwise correlation of the pressure signals with free-stream turbulence. This pressure correlation seemed to vary nearly linearly with the change in the lateral length scale of turbulence. They also observed a linear decrease in the vortex shedding correlation length with Reynolds number.

Literature also abounds with related studies on square cylinders motivated by the problem of wind-induced loading of buildings (Vickery 1966; Lee 1975; Petty 1979). Being bluff bodies, the flow over such cylinders bears some similarity to the flow over circular cylinders. Yet two features render such flows significantly different. First, the point of separation is generally fixed even though such cylinders are very prone to separation with reattachment prior to full separation. However, this behaviour is less so a function of Reynolds number than on a circular cylinder where such behaviour is occasionally observed in transitional flows. Second, the cylinder can be turned and an angle of attack associated with it. The resultant asymmetric flow does induce a steady lift force not measured on circular cylinders. Bearing these differences in mind, useful insights can be gleaned from a study such as that carried out by Vickery (1966).

Unlike other studies discussed above, Vickery measured the induced lift and drag forces on a square cylinder directly. However, it was only conducted in the Reynolds-number range 4×10^4 to $1{\cdot}6 \times 10^5$. Motivated by the problem of buffeting of large buildings, a cylinder of square cross section was used as the test cylinder. The effects of different angles of attack were investigated in detail. In spite of this, Vickery's (1966) measurements showed that for angles of attack smaller than 10°, the fluctuating lift was greatly diminished by the presence of turbulence in the free stream. Since Vickery (1966) observed that the mean drag decreased up to 30 %, in the range of Reynolds number studied, the result of the fluctuating lift measurements seemed to suggest that free-stream turbulence affects the unsteady lift in a manner similar to that of the mean drag.

Vickery's observations at low angles of attack are not unlike some preliminary data obtained by Savkar & So (1978) on a circular cylinder. The primary objective of that study was the development of the technique employed here to measure the fluctuating loads on circular cylinders immersed in a turbulent cross flow. A decrease in the fluctuating lift and drag with an increase in the free-stream turbulence was observed there, also. However, since the range of Reynolds numbers was not as extensive as the present study, the transitional character of the resulting flow, clearly identified by the present study, was not obvious in those data. In that respect, those data also indicate a functional dependence of the fluctuating lift on Reynolds numbers similar to that of the mean drag with and without turbulence in the free stream.

In view of this, the primary objective of the present study was to measure and correlate in a systematic manner the unsteady forces induced by turbulent cross flows on single rigid cylinders as a function of flow Reynolds numbers, turbulent intensity, active span-to-diameter ratio and integral length scale-to-diameter ratio. Because of the limitations in the water tunnel facility used in this investigation (see § 2.2), the

Reynolds number (based on cylinder diameter) investigated ranged from 2×10^4 to $\sim 2 \times 10^6$ (figure 1). The turbulent intensity, u'/U, where u' and U are the root-mean-square fluctuating and mean velocities along the stream direction, was set at approximately 10 % while the integral length scale-to-diameter ratio varied from 0·16 to 1·3. Finally, a range of 1 to 5·3 was selected for the active span-to-diameter ratio.

From previous studies on the Strouhal phenomenon (Jones *et al.* 1968; Loiseau & Szechenyi 1972; Richter & Naudascher 1976), it was evident that there are many discrepancies in the reported Strouhal lift coefficient. At some Reynolds numbers, the discrepancy in the reported lift coefficients is as high as a factor of three between two studies (e.g. Jones *et al.* 1968). These discrepancies are normally attributed to the fact that the experiments were carried out in different facilities with different stiffnesses for the cylinder model, that the turbulent intensity in the uniform approach stream was different (although, in general, it seldom exceeds 1 %) and that the force measurement techniques used gave different sources of errors. In view of this, it was very difficult to assess the buffeting effects by comparing the present measurements in a turbulent stream with the Strouhal measurements at the same Reynolds number reported in the literature. Therefore, it was important to obtain back-to-back Strouhal measurements to provide a correct reference for the buffeting effects. As a result, Strouhal forces were also measured and reported in the present study for the same range of parameters investigated.

This paper reports on some representative results chosen to illustrate the effects of Reynolds number and active span-to-diameter ratio on the buffeting phenomenon. It is organized into the following sections. A brief description of the experimental set-up including the water tunnel loop and the various diagnostic techniques is given in § 2. Section 3 outlines the experimental programme. A discussion of some sample force data is given in § 4. Finally, § 5 summarizes the conclusions drawn from these results.

2. Experimental set-up

2.1. *Description of the water tunnel*

The facility used in this experiment was the small water tunnel in the Applied Research Laboratory at Pennsylvania State University, State College. It is a closed-circuit tunnel and has a cross section that is circular at most points. The average velocity in the working section can be continuously varied from 0 to 24 m s^{-1} while the pressure may be reduced to 20 kPa or raised to 400 kPa independent of the water velocity in the working section. Water temperature can be maintained constant through the use of a heat exchanger or it can be allowed to rise to as high as 322 K. This feature of the tunnel is very attractive because it allows the experiment to be carried out at different water viscosities. A detailed description of this facility is given by Lehman (1959).

For the present series of experiments, the test section of the small water tunnel was replaced by a new 0·305 m diameter circular test section which was specially designed for the buffeting experiment. The test section was 1·156 m long, had a provision for introducing a turbulence-generating grid at the entrance and had three locations where the test cylinders (38·1 mm and 76·2 mm in diameter) and hot film traverse could be mounted. The test cylinders could be located at 0·254, 0·508, or 0·762 m downstream of the turbulence grid centre plane. Access holes were installed in these

locations to facilitate the installation and alignment of the test cylinders and the hot-film traverse. Caps that match with the internal curvature of the test section were used to cover up the holes and a smooth internal surface resulted. Further details of the test section can be found in the report by So (1979).

Grids of the square mesh type were designed to produce homogeneous turbulence of approximately the same intensity, but different length scale at $x/M = 10$, where x is the stream co-ordinate and M is the mesh size, in the tunnel test section. The mesh sizes chosen were 25·4, 50·8 and 76·2 mm, respectively. Square bars of different dimensions were used to make up the grid so that a blockage of $\sim 34\,\%$ results for all three grids. The estimated intensity level at $x/M = 10$ for all three grids was $\sim 10\,\%$ while the integral length scales varied from $\sim 12{\cdot}7$ mm to $\sim 50{\cdot}8$ mm. The grids were welded to frames that had circular openings of 0·305 m diameter. For the case where enhanced free-stream turbulence was not required, an empty frame was used. With this arrangement, the grids could be inserted into the box located at the entrance to the test section and could be easily changed during runs.

2.2. *Permissible flow range in the test section*

Although the water tunnel was capable of delivering a flow with a mean velocity up to 24 m s^{-1} in the test section at an operating pressure of 400 kPa, cavitation considerations at the grid and test cylinders limited the maximum mean velocity to 9·1 m s^{-1} with grids and 12·0 m s^{-1} without grids. Changing the water temperature to 322 K over the permissible velocity range had a negligible influence on these limits. Therefore, the maximum Reynolds number (based on a 76·2 mm diameter cylinder) attainable was approximately $1{\cdot}0 \times 10^6$ and 2×10^6 at 294 K and 319 K tunnel water, respectively.

2.3. *Hot film and its calibration*

To avoid cavitation problems and to maintain sufficient accuracy in the turbulence field measurements, a V-shaped wedge hot-film sensor was used because of its relatively low cavitation index compared to that of a circular cylinder (Ramamurthy & Bhaskaran 1977). The hot-film probe chosen was manufactured by DISA Electronics and had a vertex angle of approximately $\frac{1}{2}\pi$. A quartz coating 0·2 μm thick was used to cover the nickel sensors to prevent their corrosion by water. Sensor dimensions were $0{\cdot}203 \times 1{\cdot}016$ mm. The sensors had a frequency response of 0·05 Hz to 5 kHz and could resolve velocity down to $9{\cdot}1 \times 10^{-3}$ m s^{-1}. Local boiling at the surface of the sensor was eliminated by operating the hot-film probe at very low overheat ratio.

The hot-film equipment used in the present experiment consisted of the following standard commercially available units: two DISA Model 55 M01 constant-temperature anemometers, two DISA Model 55 M25 linearizers, one TSI Model 1060 true RMS voltmeter, one TSI Model 1076 digital voltmeter, and one Tektronix twin-beam oscilloscope.

The V-shaped wedge probe was mounted on a traversing rod driven by a motor capable of giving a continuous traverse at a constant speed or a manually controlled step traverse. An afterbody was inserted immediately behind the circular traversing rod to minimize probe vibrations. The afterbody was in the shape of a biconvex aerofoil, the nose of which was the circular traversing rod. With the use of two separate sets of ports, $\frac{1}{2}\pi$ apart, it was possible to traverse the flow in the test section along two orthogonal diameters.

Calibration of the sensors was carried out in the tunnel test section after the flow was checked for uniformity and axial symmetry using a pitot-static probe located at $x = 0{\cdot}508$ m downstream of the entrance. Again, an aerofoil-shaped afterbody was mounted across the tunnel behind the probe to stabilize probe vibration due to vortex shedding. The measurements were repeated along a diameter at an angle $\frac{1}{2}\pi$ from the first traverse. Results show that the flow speed was essentially identical and uniform to better than 1 % along the two diameters. The uniformity extended to as close as 12·7 mm away from the wall. Having carefully qualified the flow, the hot-film probes were calibrated in the tunnel. The calibrations covered flow velocities from 1·83 to 15·2 m s^{-1} and were repeated sufficiently often to ensure reproducibility.

2.4. *Mean drag measurements*

According to Achenbach (1968), the friction drag only contributes between 1 and 3 % to the total drag depending on the Reynolds number. This means that the total mean drag could be conveniently obtained by measuring the surface static pressure distribution around the cylinder.

Two circular cylinders (38·1 and 76·2 mm in diameter) with a smooth surface were used for the measurement of the total mean drag. Wall static pressure taps of 0·79 mm opening were drilled around the circumference of the cylinder and were distributed along a helix. A total of 33 and 29 taps, equally spaced, were used to measure the pressure distribution around the 76·2 and 38·1 mm cylinder, respectively. The cylinders could be mounted in any of the three locations in the test section and were secured in place by O rings at both ends of the cylinders.

All pressure measurements were made with respect to a total head probe located at the entrance to the inlet nozzle of the tunnel loop. A Bell and Howell Model 4-351 strain gauge-type pressure transducer with a range of $\pm$ 330 kPa was used to measure the pressure difference between the total head probe and the pressure taps on the test cylinders. The transducer output was calibrated to give a maximum reading of 20 V for 330 kPa of applied pressure. With a suitable digital voltmeter, the differential pressure could be measured to the nearest 1·72 Pa. The cylinders were aligned, as fas as possible, so that the first and the last pressure taps always read the stagnation pressure.

2.5. *Fluctuating force measurements and load-cell calibration*

To obtain information concerning the buffeting phenomenon, the effect of tube motion must be isolated from the response. The best way to achieve this is with a rigid cylinder. To be precise, a rigid cylinder is one in which the cylinder dynamic response does not significantly affect the force-response spectra. In the past, measurements of the unsteady forces were made using simple resistance-wire strain gauges. However, strain gauge techniques have one drawback: that in order to ensure reliably measurable strain, the cylinder needs to be sufficiently flexible. This conflicts with the requirement that the cylinder be rigid. In other words, there is a real danger of contamination of the results from the cylinder dynamics if the strain gauge technique is used.

This drawback was overcome by Richter & Stefan (1973) who developed a technique using piezo-electric load cells to measure the unsteady forces. Their technique was successfully used by Richter & Naudascher (1976) to measure Strouhal excitations of single cylinders in uniform cross flows. Since then, it has been extended by Savkar

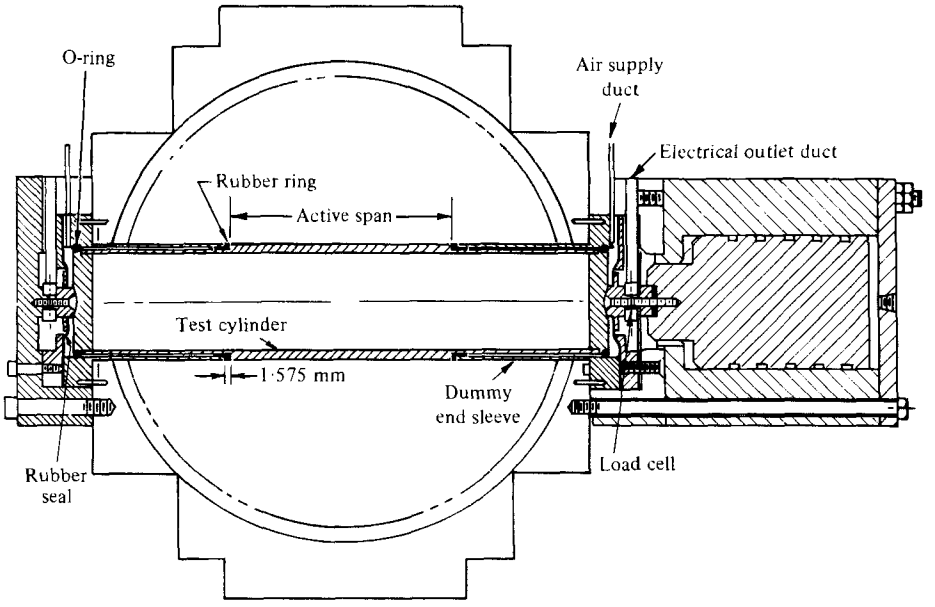

FIGURE 2. Details of test cylinder mounted across tunnel test section and location of load cells.

& So (1978) to buffeting measurements. In view of this, the latter technique was used to measure the unsteady forces in the present experiment.

Two Kistler Model 9251A piezo-electric three-axis load cells, located one at each end of the test cylinder (figure 2), were used to measure the unsteady forces. The diameters of test cylinders were 38·1 and 76·2 mm and the active span could vary from 38·1 to 203·2 mm. A pre-load of approximately 4 kN could be applied to the load cells through the pneumatic-piston device shown in figure 2. This preload also held the test cylinder in place. Since the maximum force measured was less than 0·5 kN, a pre-load-to-measured-load ratio of about 9 was achieved in the present experiments. This was higher than the ratio of 6 recommended by the manufacturer to ensure accuracy of force measurement. Four Kristal Model 5001 charge amplifiers were used to convert the load cell outputs into voltage readings and these were recorded on magnetic tape for later analysis. This arrangement allowed the fluctuating forces to be measured to the nearest 8·89 mN in the range of $\pm$ 2·67 kN. In the experiment, the load cells were oriented so that the z axis was the direction of the pre-load, while the x and r axes were aligned with the flow direction and its normal. Thus, the load cells measured the fluctuating drag along the x axis and the fluctuating lift along the r axis (figure 3).

The test cylinder assembly shown in figure 2 was modified from that used by Savkar & So (1978) to include the addition of rubber seals to separate the cylinder from the load cells, O-rings at the ends of the cylinder and rubber rings in the gap between the cylinder and the dummy end sleeves. These modifications were necessary for two obvious reasons. The first is that having water in the annular gap would have introduced added mass errors in the force measurements. Secondly, the load cells are not designed to operate in a water environment.

According to Savkar & So (1978), a natural frequency of at least four times that of

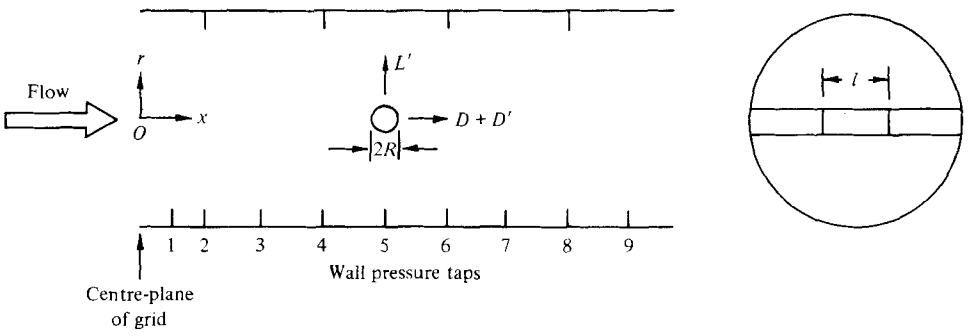

FIGURE 3. Schematic diagram of tunnel test section and wall pressure tap locations.

the dominant force frequency is required for the measurement system to work with reasonable accuracy. It was experimentally determined that the natural frequencies of the test cylinders employed in the present study were all close to 600 Hz, which was high enough to satisfy the above rule.

The calibration of the load cells was carried out statically using dead weights. It was found that within a given load cell, the calibration curves for the x and r axes, or the lift and drag axes (figure 3), were practically the same. However, due to the nature of mounting and the seals employed, the calibrations of the two load cells were measurably different. Separate calibration curves were used for the outputs of the two load cells. The level of cross-talk between the two channels was negligible. For purposes of reference, in the remainder of the paper the load cell nearest the pneumatic piston will be designated the top load cell and the one opposite the bottom load cell. To avoid introducing ambiguity in the results, the top and bottom load cells were not interchanged in the course of the study. Further, calibration checks were carried out regularly and no significant shift in the curves was noticed.

2.6. *Reliability of the load cell measurement*

Unlike pressure measurements which are carried out over a planar slice of the cylinder, the load cell gives an integrated average of the induced load over the active span. Thus, provided the spanwise correlation of the induced loading is sufficiently larger than the active span, a comparison of the results between the two measurements can be made to infer the reliability of the load cell/finite active span measurement system. When such a comparison was carried out between the Strouhal loads as measured within the present study and related measurements by Richter & Naudascher (1976) and Loiseau & Szechenyi (1972), the results were all found to be in close agreement.

2.7. *Data recording*

A Honeywell Model 5600E analogue magnetic tape recorder with fourteen input channels was used to record all measurements. The recording was carried out in FM mode at a constant speed of 15 inches per second. This gave a dynamic range of 0–5 kHz for the recorded signals. Seven channels were calibrated to accept inputs of 1 V r.m.s. and the rest were calibrated for inputs of 10 V r.m.s. All recorded signals could be checked for correctness on line.

The four load cell and two linearizer signals were modulated to give outputs of 1 V r.m.s. and are recorded as such. A seven-channel Honeywell Accudata Model

117–07 amplifier with gain factors ranging from 0·01 to 10 was used to condition these signals. In addition, a reference sine signal was generated by a Data Royal Model F230A function generator and was recorded simultaneously with the other six signals. The frequency of the reference signal was set at 2 kHz and was monitored continuously by a Hewlett Packard Model 5512A frequency counter. The Accudata amplifier, the function generator and the frequency counter all had a frequency range of 0·01 Hz to 1 MHz.

An accelerometer, attached to the wall of the test section, was used to measure the radial vibrations. This signal together with the two anemometer signals was also recorded for later analysis.

In order to ensure sufficient data for later accurate analysis, a record length of 160 s was made for each signal. As an additional precaution, a reference sine signal was recorded on all channels at the beginning of each reel of tape.

3. The experimental programme

The discussion of the experimental programme is divided into three parts. The first deals with the characterization of the flow. The second deals with the mean drag measurements and the last with the Strouhal and buffeting response.

3.1. *Characterization of the velocity field*

As with other studies (Surry 1972; Bruun & Davies 1975) the flow field is described in nominal terms in the absence of a test cylinder. To do this, the hot-film sensor was inserted at the approximate location of the test cylinder for a given x/M location with respect to the grids. However, due to the right-angled probe design, the sensor protruded about 70 mm ahead of the probe support. Consequently, the velocity measurements were actually carried out at probe locations x/M = 7·25, 8·63, 9·08 for the 25·4, 50·8, and 76·2 mm grids, respectively. For each series, the velocity traverses were carried out radially along two orthogonal radii. Detailed measurements were carried out at five locations, 50·8, 101·6, 152·4, 203·2 and 254 mm from the tunnel wall.

3.2. *Mean drag on single cylinders*

The experiment to measure the mean drag on single cylinders was carried out with the 38·1 and 76·2 mm diameter test cylinders placed at x/M = 10 (figure 3). For the no-grid case, the test cylinders were placed at x = 0·508 m.

In order to increase the Reynolds number to 2×10^6, another set of measurements was obtained with water temperature elevated 319 K from the normal condition of 294 K and the maximum allowable flow. This series of runs was not very successful with the 38·1 mm diameter cylinder because the high water temperature caused the Tygon tubing to expand and loosen from the pressure taps. Consequently, the high-temperature run was only carried out on the 76·2 mm diameter cylinder.

3.3. *Fluctuating forces on single rigid cylinders*

The test cylinders for the fluctuating force measurements were installed at x/M = 10 with turbulence grids placed at the tunnel entrance and at x = 0·508 m when there was no grid (figure 3). Water temperature was maintained at 294 K. Five different cylinder geometries were tested for each grid configuration and flow condition. These were: 76·2 mm active span for the 76·2 mm diameter cylinder and 38·1, 76·2, 114·3 and 203·2 mm active spans for the 38·1 mm diameter cylinder.

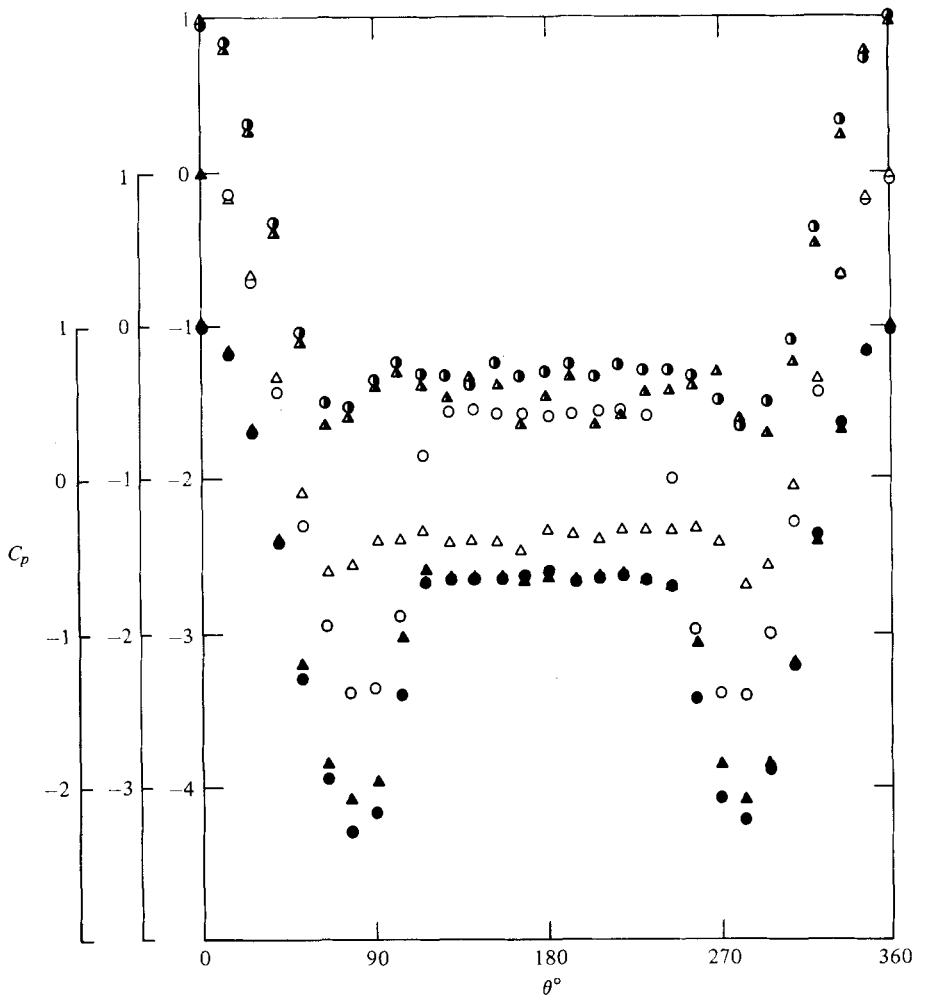

FIGURE 4. Pressure distributions around the 38·1 mm diameter test cylinder in cross flows at three different Re. With no grid: ▲, $Re = 2{\cdot}62 \times 10^4$; △, $Re = 10{\cdot}0 \times 10^4$; ▲, $Re = 30{\cdot}6 \times 10^4$. With 50·8 mm grid: ◑, $Re = 2{\cdot}67 \times 10^4$; ○, $Re = 10{\cdot}4 \times 10^4$; ●, $Re = 34{\cdot}5 \times 10^4$.

The high-Reynolds-number runs were again carried out with the water temperature elevated to 319 K. Since no problems developed, runs were made for all four different grids and five different cylinder geometries at maximum flow setting.

4. Discussion of results

The purpose of this paper is to examine the effects of free-stream turbulence and Reynolds number on the steady and fluctuating forces acting on single rigid cylinders in cross flows. In addition, it reports on the results of varying the active span of the test cylinders on the buffeting forces. The effects of changing the integral length scale of the approach flow, the correlation of the fluctuating force spectra with the upstream velocity spectrum and other detailed analyses of the measurements will be reported in the future. In view of this, the flow measurements reported here are limited to the mean velocity and turbulent intensity.

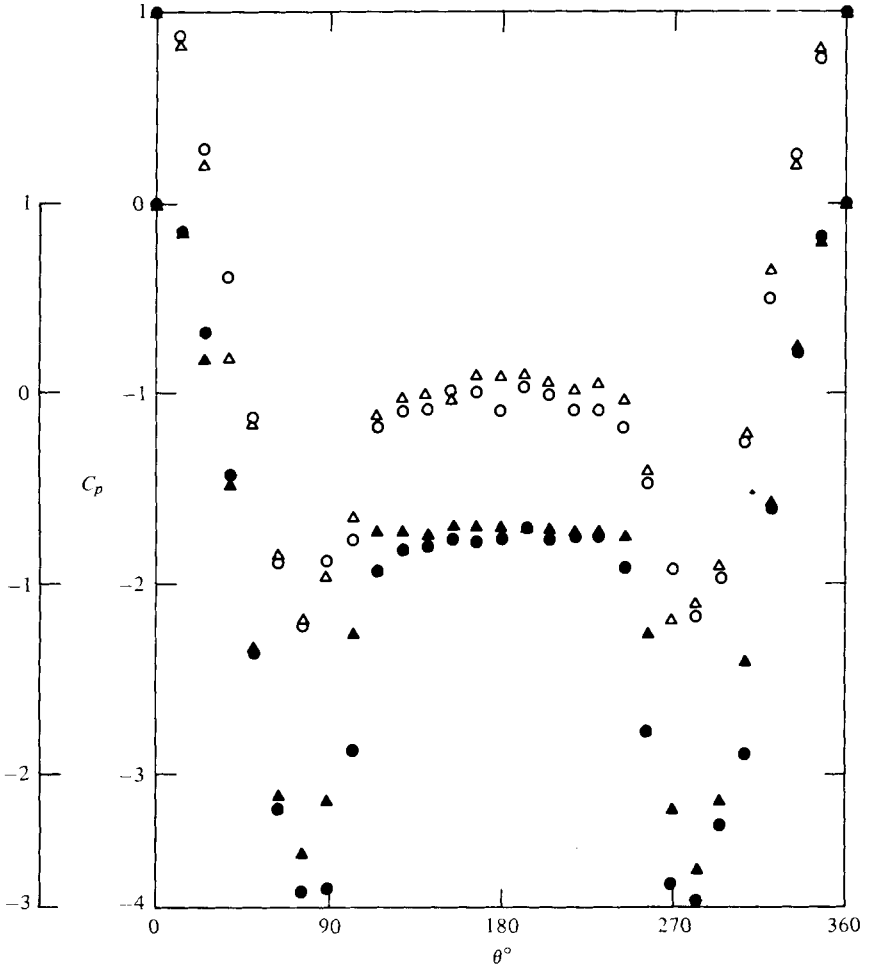

FIGURE 5. Pressure distributions around the 38·1 mm diameter test cylinder in cross flows at two different Re. With 25·4 mm grid: △, $Re = 5{\cdot}48 \times 10^4$; ▲, $Re = 30{\cdot}44 \times 10^4$. With 76·2 mm grid: ○, $Re = 5{\cdot}96 \times 10^4$; ●, $Re = 27{\cdot}78 \times 10^4$.

The mean velocity, U, and the turbulent intensity, u'/U, were obtained by passing the recorded linearized signals through an analogue sum and difference amplifier and then through a true r.m.s. meter. Thus determined, U was found to be very uniform across a diameter of the tunnel, at least within the range that extends from 50·8 to 254 mm away from the tunnel wall. The results for the no-grid, 25·4, 50·8, and 76·2 mm grid cases were essentially identical. As for the turbulent intensity, u'/U was measured to be 0·5 % with a variation of 0·07 % for the no-grid case. When the three different grids were installed at the tunnel entrance, u'/U measured at the nominal $x/M = 10$ location was found to be 9·5 % ± 1 %. The variation across the tunnel was less than the 1 % variation obtained by changing the grids. Consequently, the turbulent intensity produced by the three different grids at $x/M = 10$ can be considered identical and is taken to be 9·5 %.

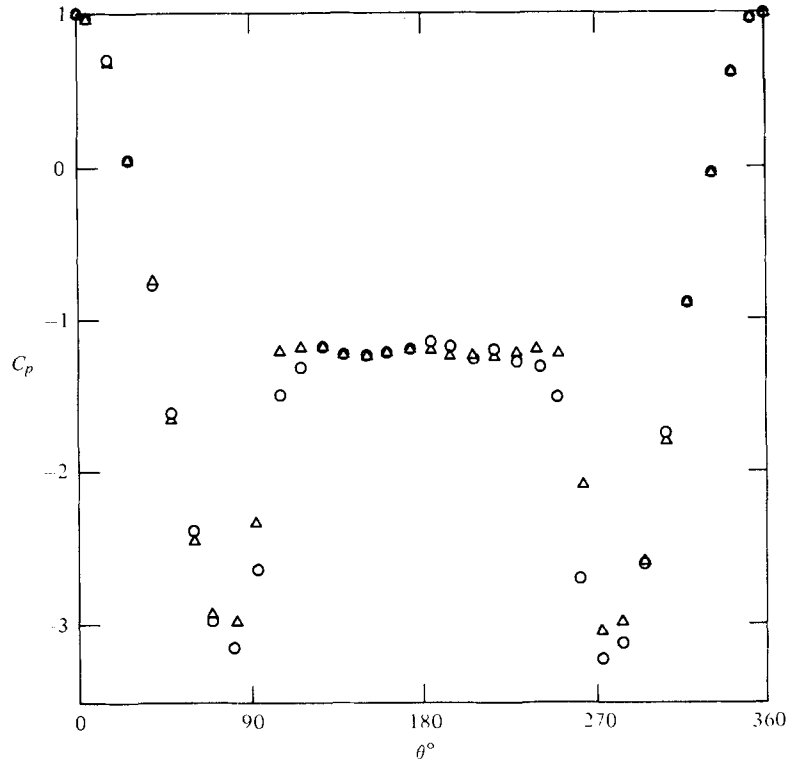

FIGURE 6. Pressure distributions around the 76·2 mm diameter test cylinder in uniform and turbulent cross flows. △, $Re = 82{\cdot}1 \times 10^4$, no grid; ○, $Re = 68{\cdot}0 \times 10^4$, 50·8 mm grid.

4.1. *Mean drag*

Sample plots of the C_p distribution around a single cylinder in uniform as well as turbulent cross flows are given in figures 4–6. These plots were chosen to illustrate the similarity or difference in the pressure distribution around the cylinder when it was exposed to uniform and turbulent cross flows at about the same Reynolds number. Figure 4 shows the distributions for the 38·1 mm diameter cylinder at three different Reynolds numbers in a uniform stream and a turbulent stream created by the 50·8 mm grid. The turbulent intensities for these two streams were 0·5 % and 9·5 %, respectively. It can be seen that at pre-transitional Reynolds number ($2{\cdot}6 \times 10^4$), the 9·5 % turbulent intensity in the approach flow does not significantly disturb the boundary-layer development around the cylinder. As a result, a laminar separation of the viscous layer still occurs, and approximately the same C_p distribution is obtained for the two cases (figure 4). As the Reynolds number, Re, is increased to approximately 10^5, a laminar separation of the viscous layer still persists in the uniform flow case, but the separation seems to change to a turbulent one for the turbulent flow case. This gives rise to a big difference in the base pressure between the two cases, with the base pressure being higher in the case of a turbulent cross flow (figure 4). Further increase in Re to 3×10^5 causes the viscous layer to have a turbulent separation in the uniform flow case, too, and the C_p distributions for the two cases, with or without the grid, are again identical (figure 4). Changing the grids but not the turbulent intensity does not have an

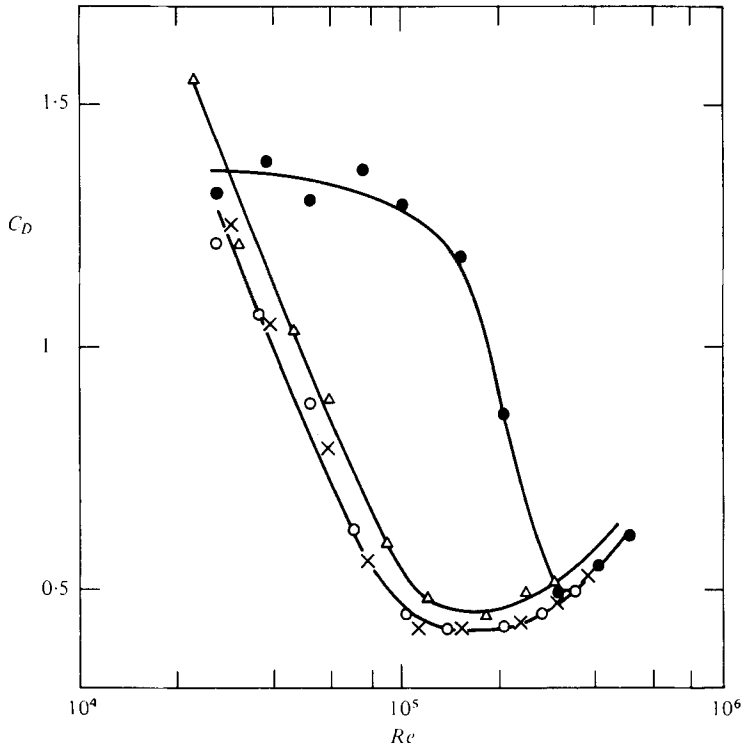

FIGURE 7. Mean drag variation with Re for the 38·1 mm diameter test cylinder in uniform and turbulent cross flows. ●, no grid; ×, 25·4 mm grid; ○, 50·8 mm grid; △, 76·2 mm grid.

appreciable effect on the general development of the flow and essentially the same C_p distributions are obtained at the same Re for turbulent cross flows created by different grids (figure 5). Increasing the blockage effects by changing to a 76·2 mm diameter cylinder does not alter the flow picture much, except to decrease the base pressure (figure 6). Therefore, the effects of free-stream turbulence are to cause the viscous layer around the cylinder to transit from laminar to turbulent at a lower Reynolds number. This is reasonable because with a turbulent upstream, additional energy is available from the turbulence field to energize the boundary layer and cause the layer to have a natural transition from laminar to turbulent at a lower Re. In the absence of upstream turbulence, the layer has to acquire the additional energy from the approach flow in the form of higher Re before transition to turbulent flow occurs.

From the above discussion, it can be expected that the mean drag on the cylinder is essentially the same for both uniform and turbulent cross flows at pre-transitional Reynolds numbers. This is shown in figures 7 and 8 where the C_D for the 38·1 and 76·2 mm diameter cylinders are plotted *vs.* Re for the four different grids tested. Although the measured Re is not quite in the pre-transitional range for the turbulent flow cases, the resultant C_D variations with Re appear to indicate that the mean drag on the cylinder may approach the same value at some pre-transitional Re for both uniform and turbulent cross flows. One obvious exception is the C_D distribution for the 38·1 mm diameter cylinder in a turbulent cross flow produced by the 76·2 mm grid (figure 7). Here the C_D is consistently higher than those obtained with the other two grids. Since the blockage is the same, one possible reason for the discrepancy is the effect of the

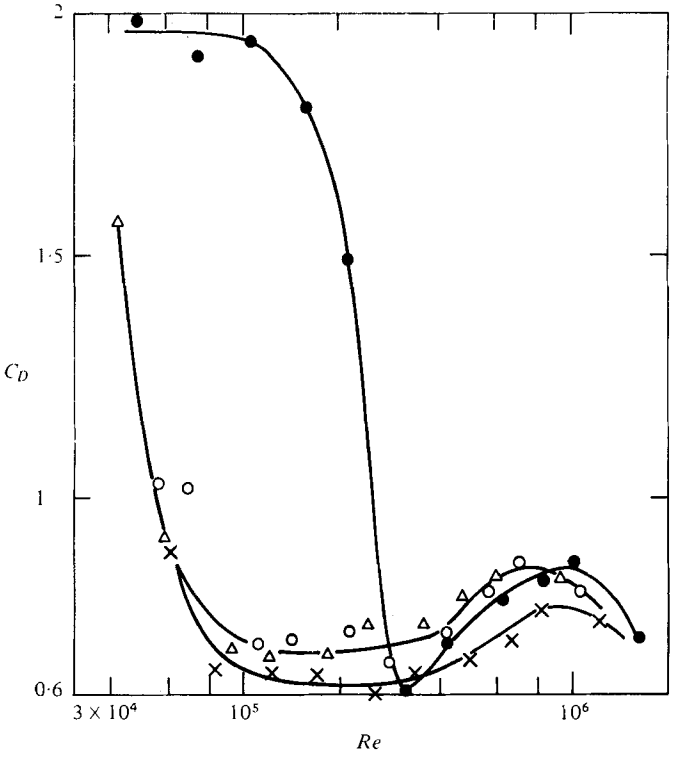

FIGURE 8. Mean drag variation with Re for the 76·2 mm diameter test cylinder in uniform and turbulent cross flows. ●, no grid; ×, 25·4 mm grid; ○, 50·8 mm grid; △, 76·2 mm grid.

integral length scale-to-diameter ratio. For the 76·2 mm grid case, this ratio is largest and is estimated to be greater than one. On the other hand, the integral length scale-to-diameter ratio for the same cylinder exposed to turbulent flows generated by the 25·4 and 50·8 mm grids is estimated to be less than one. This difference in integral length scale-to-diameter ratio could contribute to the observed difference in C_D at the same Re. It is hoped that when all the data are analysed, evidence in support of this hypothesis can be found.

The effects of blockage on C_D are summarized in figure 9, where the present results for uniform flow are compared with the 25 % blockage data of Richter & Naudascher (1976) and zero blockage measurements of Wieselsberger (1923). Present results are consistent with other measurements at pre-transitional Re in that increased blockage results in increased C_D. Wide discrepancies occur at transitional Re, but then other measurements reported in the literature do not agree either (Achenbach 1968). The disagreement is normally attributed to such factors as span-to-diameter ratio, surface roughness, small free-stream turbulence intensity level (anywhere from 0 to 1 %), tunnel inlet conditions, etc.

The main purpose of this paper is to examine the buffeting forces; therefore, the C_D data presented are not corrected for blockage. In spite of this, it can be assumed that blockage does not significantly affect the trends in the data (figure 9), although the absolute magnitudes are obviously highly dependent on the blockage.

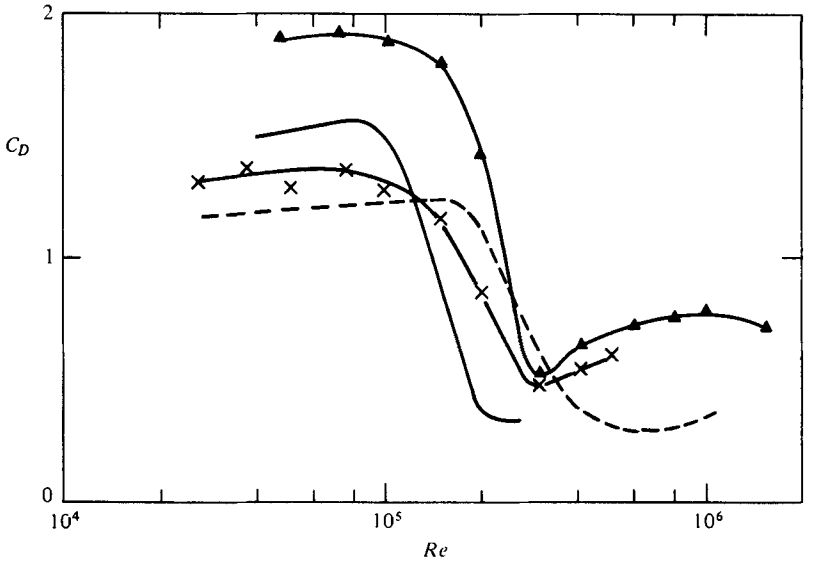

FIGURE 9. Effects of tunnel blockage on mean drag variation with Re for single cylinders in uniform cross flows. Present measurements: ×, ▲, 16 and 32 per cent blockage, respectively. Other measurements: - - -, zero blockage, Wieselsberger (1923); ——, 25 per cent blockage, Richter & Naudascher (1976).

4.2. *Fluctuating forces*

The choice of data to be reported here was partially guided by the desire to establish the credibility of the present experimental set-up and measurement technique. Since the Strouhal measurements of Richter & Naudascher (1976) were also obtained by a similar force measurement technique, it is worthwhile to compare their data with the present Strouhal measurements. To preclude spurious conclusions, this comparison was carried out for the case where the active span-to-diameter ratio of the two studies was large (preferably $\geqslant 3$). The cylinder used by Richter & Naudascher (1976) had an $l/2R = 6{\cdot}77$ where l is the active span and $2R$ is the cylinder diameter. Therefore, the 38·1 mm diameter by 114·3 mm active span cylinder measurements were selected from the present work. Buffeting data obtained under conditions where the integral length scale-to-diameter ratio is of order one were selected. These considerations, therefore, lead to the selection of the following set of data to illustrate the effects of free-stream turbulence, Reynolds number and active span-to-diameter ratio on the fluctuating forces. The data set was selected from runs made on the 38·1 mm diameter test cylinders and they include:

(*a*) Strouhal forces (lift and drag) for the 114·3 mm active span,

(*b*) buffeting forces (lift and drag) for the 114·3 and 203·2 mm active span due to a 50·8 mm grid, and

(*c*) buffeting lift force only for the 38·1 and 76·2 mm active span due to a 50·8 mm grid.

The summary data presented are mainly the r.m.s. forces. However, some representative auto-power spectra, probability density functions and other statistics are also presented.

The force signals were fed into a Krohn-Hite Model 3322 filter before inputting into

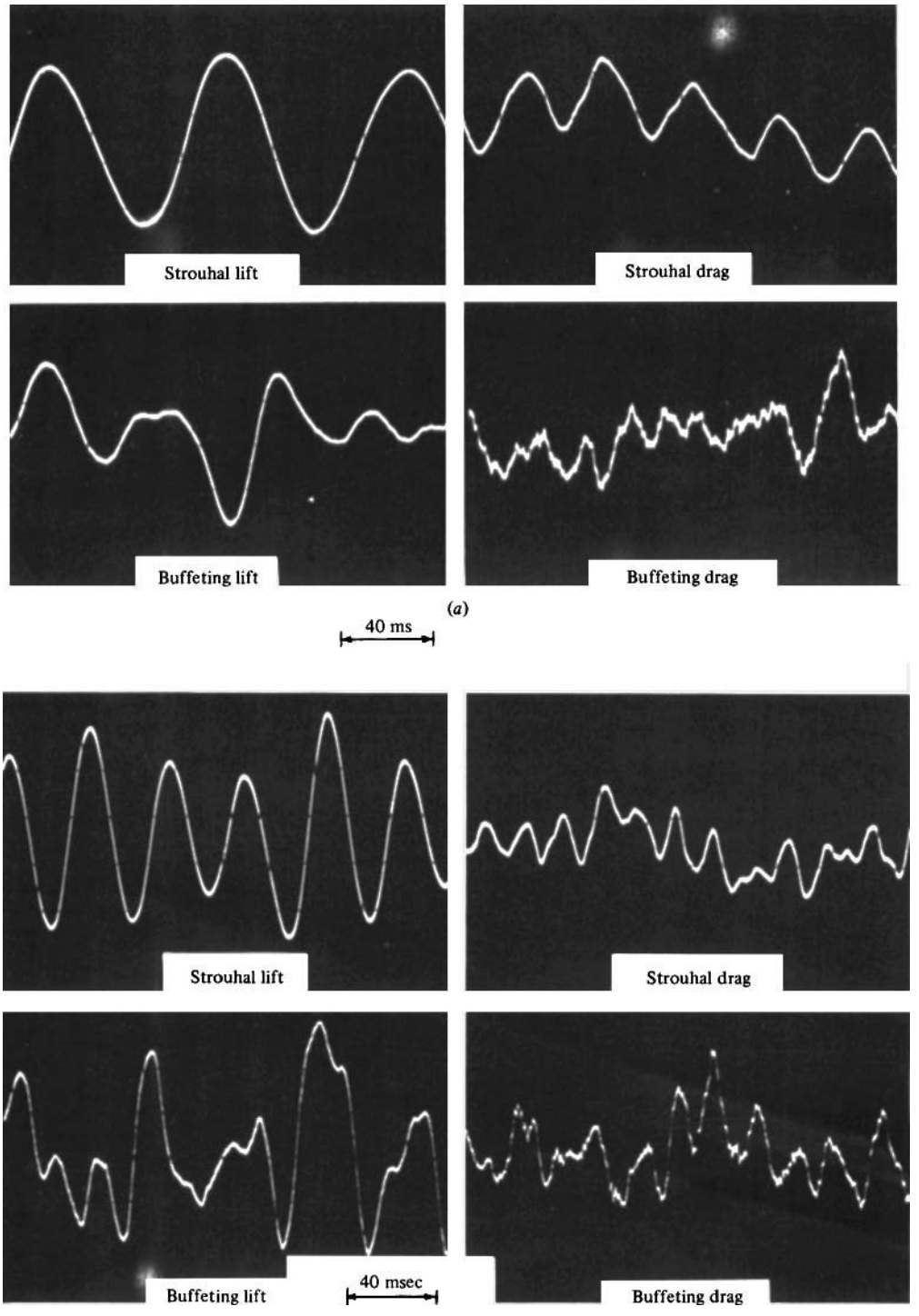

FIGURE 10 (*a*, *b*). For legend see p. 413.

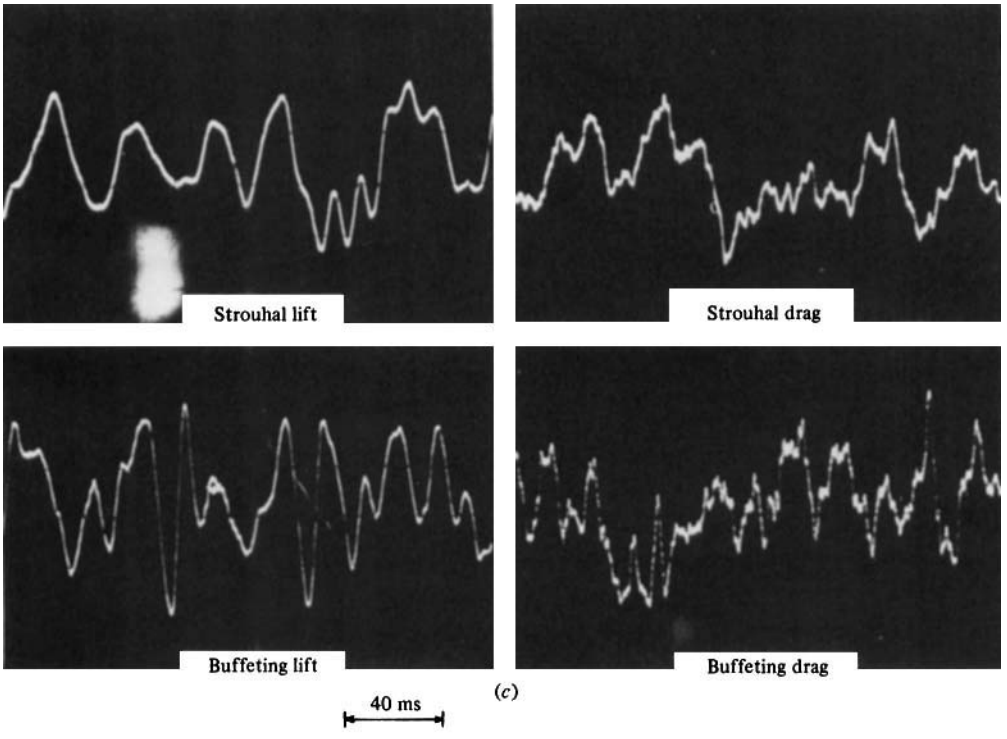

FIGURE 10. Traces of Strouhal and buffeting forces for the 114·3 mm active span test cylinder at three different Reynolds numbers. (*a*) $Re \sim 1 \times 10^5$; (*b*) $Re \sim 2 \times 10^5$; (*c*) $Re \sim 3 \times 10^5$.

a Hewlett-Packard Model 5451A Fourier analyser for auto-power spectrum and statistical calculations. Since Strouhal frequencies as low as 3 Hz were measured, the bandwidth chosen for the filter was 0·01 Hz to 1 kHz. The integral of the auto-power spectra gave the mean square values of the unsteady lift and drag forces. Since the accuracy of these values depends to a large extent on such parameters as total time period, sampling rate, etc., chosen for the digital data analysis, their proper choice is important (Bendat & Piersol 1971). These parameters were chosen to give an accuracy of $\pm 6\,\%$ on the calculated mean square lift and drag and a maximum frequency high enough to resolve the auto-power spectrum to at least two decades down in a log–log plot of the spectrum versus frequency. As a check, the filtered signals were also passed through a true r.m.s. meter to determine the mean square lift and drag.

Finally, the probability density functions of the signals were determined by passing the filtered signal through a 400-line SAICOR Model ASI-43A Correlator and Probability Analyzer.

(*a*) *Characteristics of the fluctuating forces.* The time signals of the Strouhal and buffeting forces induced on the 114·3 mm active span cylinder are shown in figure 10. Three representative *Re* are selected to illustrate the changing nature of the force signals. The time base for all the traces shown is the same but the vertical voltage scale is not. Therefore, the traces can be compared for their frequency characteristics only. This set of three traces were obtained from the bottom load cell. Similar traces were also obtained from the top load cell. Since these traces all give the same unsteady

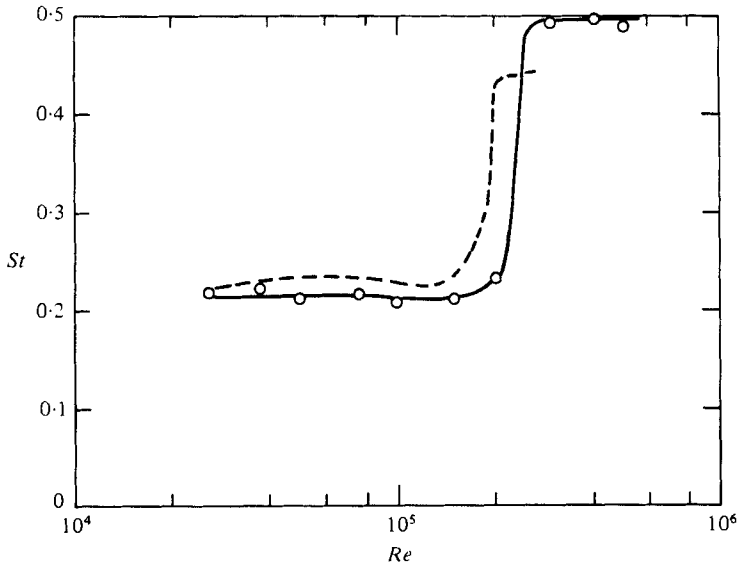

FIGURE 11. Variation of St with Re. Measurements: ○, $l/2R$ = 3·0; - - -, $l/2R$ = 6·77, Richter & Naudascher (1976).

forces, only one set is presented here for discussion purposes. More will be said about the measured forces obtained from the top and bottom load cells later.

The set of traces clearly show the effects of turbulent intensity on the induced forces, since the intensity level was 0·5 % for the uniform flow and 9·5 % for the flow generated by a 50·8 mm grid. At $Re \simeq 10^5$ (figure 10a), it can be seen that both the Strouhal lift and drag signals are periodic. However, the frequency of the drag signal is twice that of the lift. In spite of this similarity, the amplitude of the drag signal appears to be slightly modulated while this is not observed in the lift signal. On the other hand, the buffeting lift and drag signals at the same Re are more representative of narrow- and wide-band random signals (figure 10a). In spite of this, a distinct frequency could be identified for the buffeting lift, and its Strouhal number appears to be about 0·3. As the Reynolds number is increased to 2×10^5, the Strouhal lift still shows a distinct frequency but there appears at the same time a modulation to the amplitudes (figure 10b). The Strouhal drag signal becomes more and more random and so are the buffeting lift and drag signals. In addition, high-frequency fluctuations are noticeable in the buffeting drag (figure 10b). Further increase in Re to 3×10^5 brings out the randomness in the Strouhal lift signal and no distinct frequency can be easily identified (figure 10c). At the same time, more and more high-frequency fluctuations are noticeable in the Strouhal drag and buffeting lift and drag signals.

This series of events strongly suggests that the Strouhal forces go through a transition region where the forces change from a highly organized nature to a purely random one. The organized nature is indicative of the orderly alternate shedding of vortices due to laminar separation of the viscous layer from the cylinder surface. As the Reynolds number is increased to the transitional value, the excursion of the separation point becomes larger and the strength of the shed vortices would begin to vary. The result of this is reflected in the changing amplitude of the Strouhal lift.

(*b*) *Strouhal frequency.* The Strouhal frequencies of the lift and drag signals were

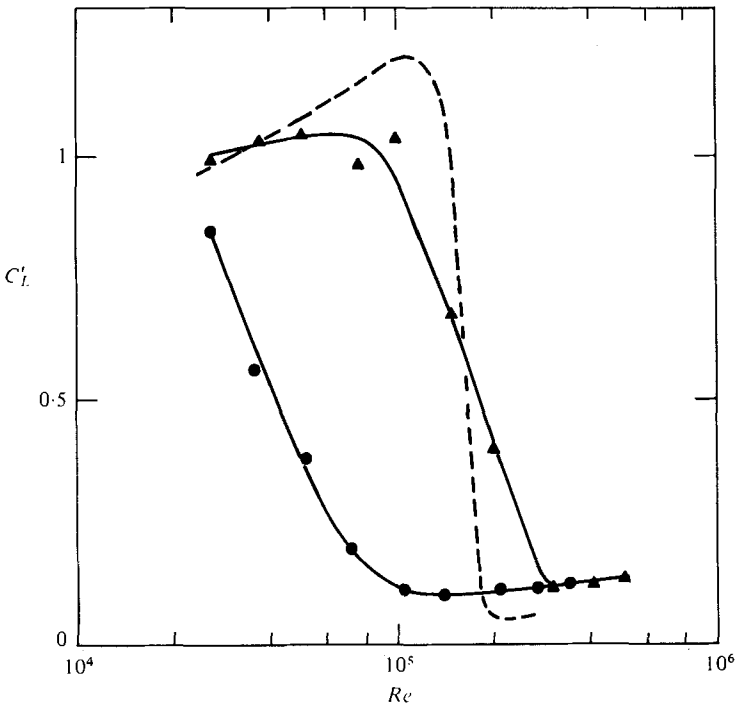

FIGURE 12. Variation of the fluctuating lift coefficients with Re for the 114·3 mm active span test cylinder. Present measurements: ▲, Strouhal lift; ●, buffeting lift due to a 50·8 mm grid. Other measurements: – – –, Strouhal lift by Richter & Naudascher (1976). The $l/2R$ ratio for these measurements is given in figure 11.

determined from the auto-power spectra of the signals. At low Re, the lift and drag spectra are similar to those obtained by Richter & Naudascher (1976). Therefore, they are not shown here. There is only one distinct peak in the spectra and the Strouhal frequencies can be identified without ambiguity. As Re is increased, the peak in the spectra becomes less and less distinct, resulting in no identifiable peak for the Strouhal drag at $Re = 3 \times 10^5$. The calculated Strouhal number, $St = f_L 2R/U$, is plotted versus Re in figure 11. It can be seen that St remains fairly constant at 0·21 for Re less than 2×10^5 but increases to approximately 0·5 abruptly for $Re \geqslant 3 \times 10^5$. The data of Richter & Naudascher (1976) with 25 % blockage are also included in figure 11 and show good agreement.

According to a recent study by Loiseau & Szechenyi (1972), the sudden increase in St can be attributed to the appearance of a prominent peak in the force spectrum at about twice the shedding frequency. They explained this by noting that it does not represent a shift in the normal shedding frequency but rather represents a different phenomenon altogether. The phenomenon is associated with the well-known existence of double-frequency pressures in the vicinity of the trailing edge because of alternate vortex shedding from the cylinder. At pre-transitional Re, the vortex shedding is regular and the pressure fields induced at these frequencies on either side of the cylinder are well correlated and therefore cancel each other. However, at transitional Re, vortex shedding is random and irregular. As a result, the pressures on either side of the

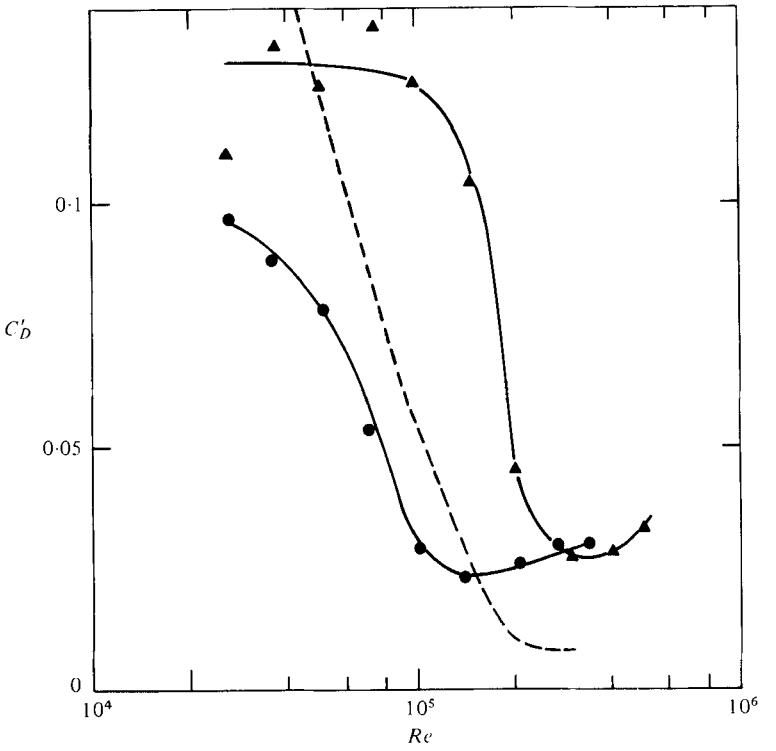

FIGURE 13. Variation of the fluctuating drag coefficients with Re for the 114·3 mm active span test cylinder. Legend same as for figure 12.

cylinder are no longer well correlated and hence do not cancel. This, therefore, gives rise to a net lift at the double frequency. Although this may appear dominant in the lift spectrum, it should not be confused with the shedding frequency. If the shedding frequency at transitional Re is taken to be half the frequency determined from the peak in the lift spectrum, then the resultant St would again assume a constant value of approximately 0·2. It is hoped that, when all the measurements are analysed, further evidence in support of this argument can be obtained.

(*c*) *Effects of turbulent intensity and Reynolds number.* The r.m.s. Strouhal and buffeting lift and drag coefficients are defined as

$$C'_L = \frac{L'}{\rho U^2 l R}, \quad C'_D = \frac{D'}{\rho U^2 l R},$$

where ρ is the fluid density, L' and D' are the total r.m.s. fluctuating lift and drag measured by both the top and bottom load cells. It will be shown later that each load cell indeed measures one-half of the total forces acting on the cylinder. Therefore, in the calculation of C'_L and C'_D, L' and D' can be taken to be twice the values determined from either the top or bottom load cell. The results shown in figures 12–16 were obtained by passing the bottom load cell signals through a true r.m.s. meter.

The variations of both the Strouhal and buffeting C'_L and C'_D with Re are shown in figures 12 and 13, respectively. In addition, the Strouhal C'_L and C'_D from Richter & Naudascher's (1976) 25 % blockage data are also shown for comparison. Bearing in

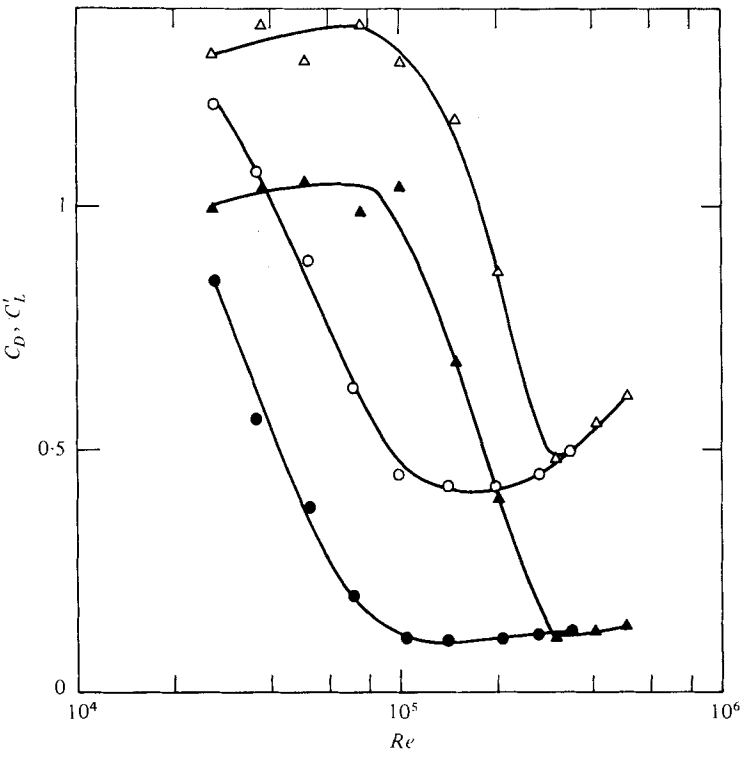

FIGURE 14. A comparison of the behaviour of the mean drag and fluctuating lift coefficients for the 114·3 mm active span test cylinder in uniform and turbulent cross flows. With no grid: △, C_D; ▲, C'_L. With 50·8 mm grid, ○, C_D; ●, C'_L.

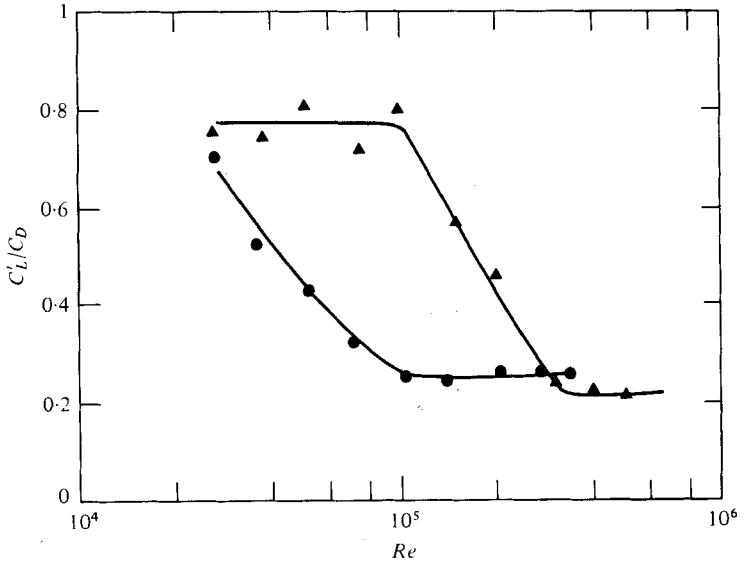

FIGURE 15. Variation of the Strouhal and buffeting C'_L/C_D ratio with Re. ▲, no grid; ●, 50·8 mm grid.

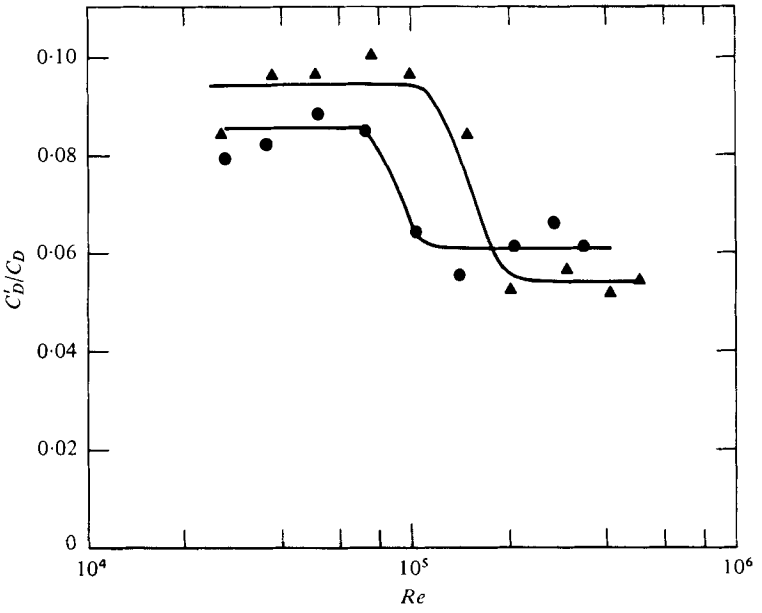

FIGURE 16. Variation of the Strouhal and buffeting C_D'/C_D ratio with Re. ▲, no grid; ●, 50·8 mm grid.

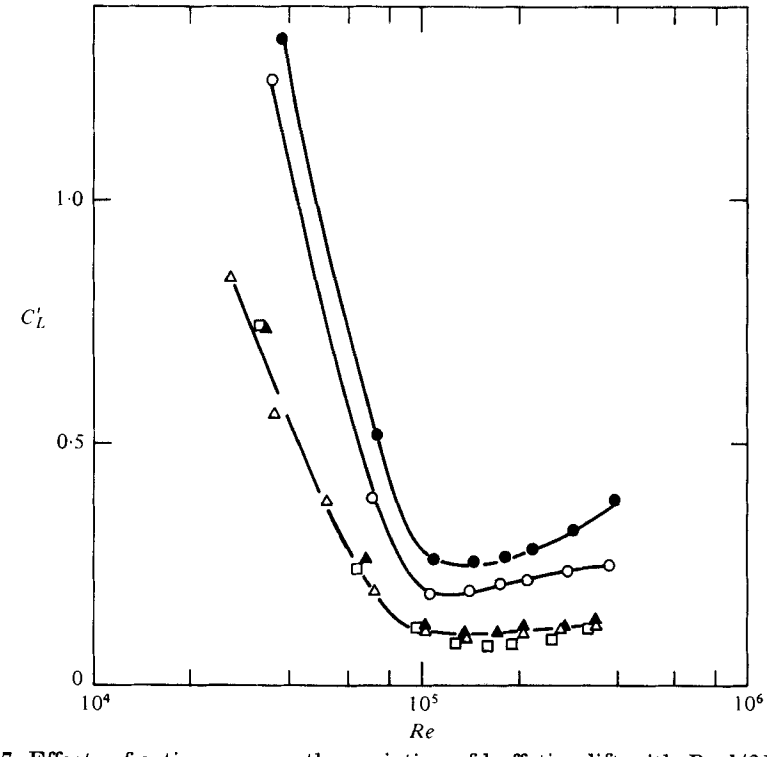

FIGURE 17. Effects of active span on the variation of buffeting lift with Re. $l/2R$: ●, 1; ○, 2; ▲, 3; □, 5·3 (data based on top load-cell measurement); △, 3 (data based on bottom load-cell measurement).

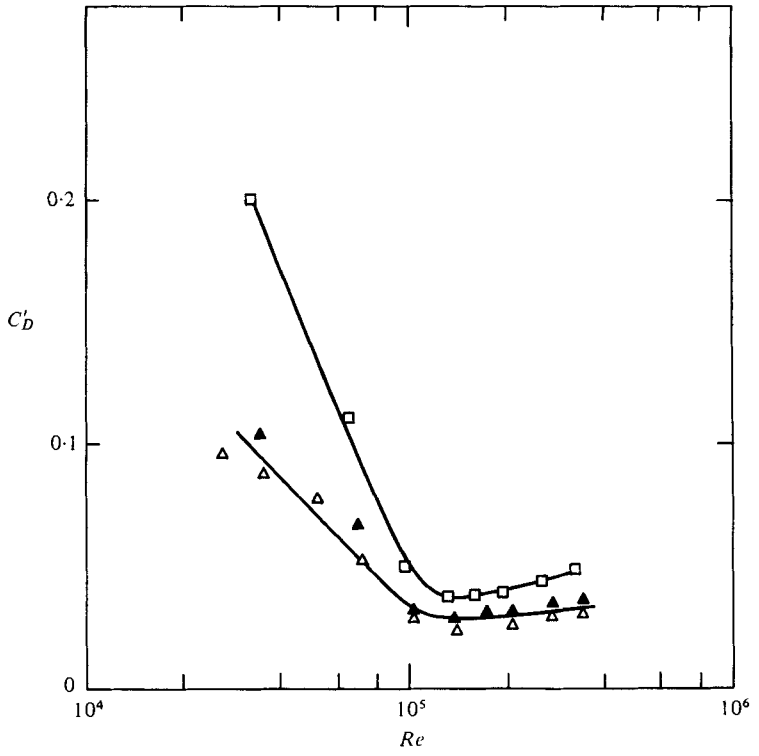

FIGURE 18. Effects of active span on the variation of buffeting drag with *Re*. For legend see figure 17.

mind that there is widespread discrepancy in the Strouhal C'_L at transitional *Re* (see Loiseau & Szechenyi 1972; Jones *et al.* 1968), the agreement between the present measurements and those of Richter & Naudascher (1976) shown in figures 12 and 13 is rather remarkable. The major importance of figures 12 and 13, however, is the behaviour of the C'_L and C'_D curves and the effects of turbulent intensity on the fluctuating forces. Both the Strouhal C'_L and C'_D go through a transition region where the values drop tenfold for the Strouhal C'_L (figure 12) and fivefold for the Strouhal C'_D (figure 12). The same behaviour is observed for the buffeting C'_L and C'_D; however, the transition occurs at a lower range of *Re*. This similarity between the behaviour of the fluctuating forces and that of C_D with *Re* is an important observation.

A most convincing illustration of this similarity can be found in figure 14, where the mean drag and the fluctuating lift forces are plotted *vs.* *Re* for the no-grid and 50·8 mm grid cases. The effects of turbulent intensity are to shift the transition region to a lower *Re* range, and they are clearly evident for both the C_D and C'_L curves. In addition, the two sets of curves are very similar and the corresponding values of C_D and C'_L are about the same, with C'_L slightly smaller than C_D for the range of *Re* tested. This suggests that for design purposes, a conservative estimate of the C'_L can be obtained from the C_D versus *Re* curves for both Strouhal and buffeting forces.

The fact that the fluctuating forces do not exceed the mean drag for the range of *Re* tested is best illustrated by examining figures 15 and 16 where the ratios C'_L/C_D and C'_D/C_D are plotted against *Re*. It can be seen that C'_L/C_D varies from 0·8 to 0·2 for both

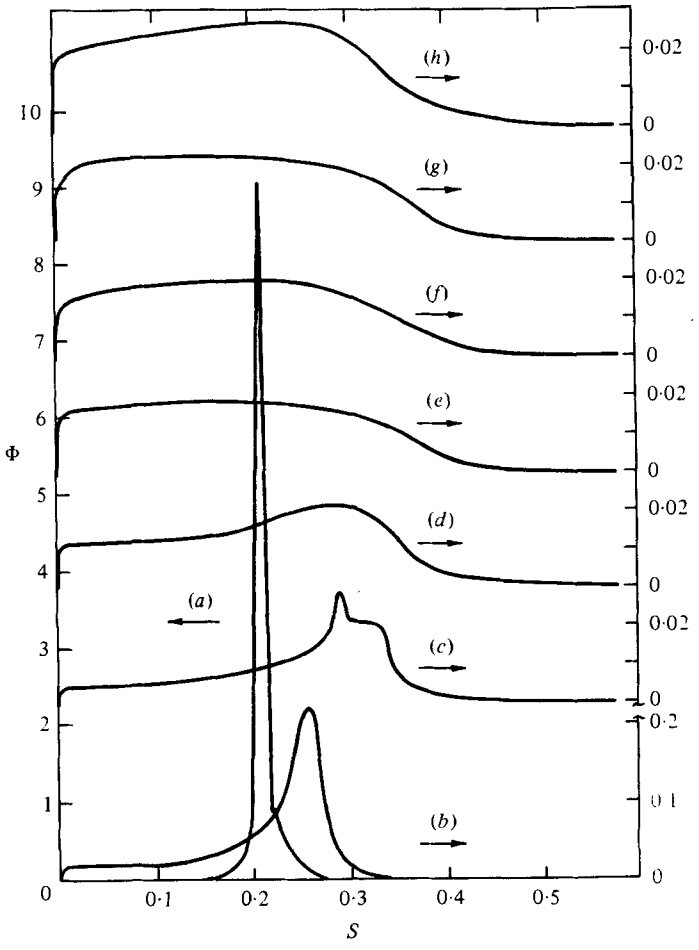

FIGURE 19. The power spectral density function of buffeting lift at different Re for the 114·3 mm active span test cylinder. $Re \times 10^{-4}$: (*a*) 3·45; (*b*) 6·89; (*c*) 10·34; (*d*) 13·79; (*e*) 17·31; (*f*) 20·71; (*g*) 27·62; (*h*) 34·51.

Strouhal and buffeting forces (figure 15) while C_D'/C_D varies from 0·1 to 0·05 for the Strouhal drag and from 0·08 to 0·06 for the buffeting drag (figure 16).

(*d*) *Stationary nature of the buffeting forces.* In order to demonstrate that the measured buffeting forces are stationary and the two load cells are indeed measuring equal loads, a duplicate run on the 38·1 mm cylinder with an active span of 114·3 mm was carried out with the 50·8 mm grid installed at the tunnel entrance. The recorded buffeting data from the top load cell have been analysed and compared with the results shown in figures 17 and 18. This time, a detailed analysis of the force signals was carried out and the C_L' and C_D' were calculated from different segments of the recorded signals. The calculated C_L' and C_D' from different load cells and different segments of the recorded signals are in agreement with each other to within $\pm$ 6 %. This shows that the buffeting forces are indeed stationary and the measured mean square forces are reproducible. Results from one run showing the data from both load cells are shown as open and closed triangular symbols in figures 17 and 18. It can be seen that, to within measurement and data analysis error, the two sets of results are essentially the same.

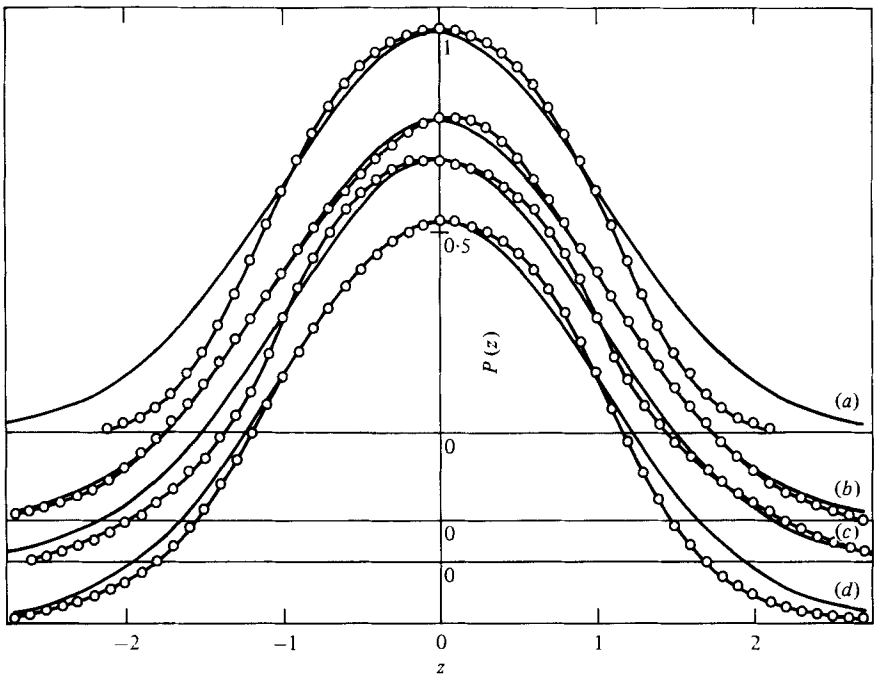

FIGURE 20. The probability density function of buffeting lift and drag at two different Re for the 114·3 mm active span test cylinder. $Re = 3{\cdot}45 \times 10^4$: (*a*) lift; (*b*) drag. $Re = 34{\cdot}51 \times 10^4$: (*c*) lift; (*d*) drag. ——, Gaussian random signal.

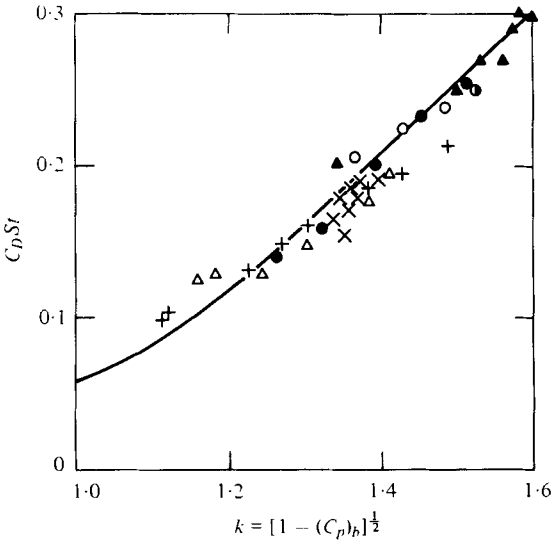

FIGURE 21. Variation of $C_D St$ with base pressure parameter k. Uniform flow data: ×, Roshko (1961); +, Bearman (1967); ◑, Surry (1972); ▲, present measurements. Turbulent flow data: △, Bearman (1967); ○, Surry (1972); ●, present measurements. ——, theoretical curve, Bearman (1967).

It follows that the two load cells do measure equal load, and the unsteady forces can be correctly resolved by considering the output from either the top or bottom load cell only.

(*e*) *Effects of span-to-diameter ratio on buffeting forces.* Figures 17 and 18 also show the effects of span on C_L' and C_D'. The outputs from the top load cell of the 38·1, 76·2, and 203·2 mm active span cylinder runs are plotted. It can be seen that as the active span is increased, a lower value of C_L' is obtained at the same Re. According to Schmidt (1970) and Loiseau & Szechenyi (1972), this decrease in C_L' is a direct consequence of the less than perfect correlation of the lift force as the span is increased.

(*f*) *Other properties of the buffeting forces.* The spectra of the buffeting lift are generally similar for the four different active spans tested. Therefore, only one set of spectra for the Re range investigated are shown. The set chosen is the 114·3 mm active span run. Since the Hewlett-Packard Fourier Analyzer gives the auto-power spectrum $E(f)$, in V^2, and the frequency, f, in Hz, the calculated spectra are reduced to a normalized form for presentation. To do this, consider the relation for the mean-square lift coefficient

$$C_L'^2 = \frac{L'^2}{(\rho U^2 lR)^2} = \int_0^\infty \frac{E(fD/U)}{(\rho U^2 lR)^2} \frac{U}{2R} d\left(\frac{2R}{U} f\right).$$

This suggests that $E(f)$ and f should be normalized with respect to $(\rho U^2 lR)^2/(U/2R)$ and $U/2R$. Denoting the dimensionless quantities by Φ and S where

$$\Phi = \frac{(U/2R)\, E(2fR/U)}{(\rho U^2 lR)^2}, \quad S = \frac{2fR}{U},$$

the calculated spectra are plotted in figure 19 for the Re range $3{\cdot}45 \times 10^4$ to $34{\cdot}51 \times 10^4$. It can be seen that at low Re the force response is Strouhal-like. However, as Re increases, a slow broadening of the spectrum is observed. At $Re = 13{\cdot}79 \times 10^4$, the distinct peak in the spectrum disappears, and thereafter the spectral response resembles that of the upstream turbulent flow. Also, note the reduction in amplitude of the peak. From a high of $\Phi \cong 9$ at $Re = 3{\cdot}45 \times 10^4$, it reduces to $\Phi \cong 0{\cdot}02$ at $Re = 13{\cdot}79 \times 10^4$. This is consistent with the large decrease in C_L' shown in figure 12.

Since the skewness and kurtosis of a Gaussian random signal are zero and 3, respectively, and the corresponding values for a sine wave are zero and 1·5, the calculated skewness and kurtosis of the buffeting lifts will indicate the periodic nature of the forces. The result of this calculation shows that the skewness of the buffeting lift force is essentially zero. It varies from a low of $-0{\cdot}014$ to a high of 0·043. There is no identifiable pattern for this variation in terms of either the active span or the Re. On the other hand, the kurtosis varies from a value of 2·53 at the lowest Re to a value of 3·34 at the highest Re investigated. It increases with Reynolds number up to $Re \simeq 1{\cdot}5 \times 10^5$. Beyond that, the kurtosis remains fairly constant at $3{\cdot}13 \pm 0{\cdot}2$. Much the same variation is true for all active spans investigated. This shows that the character of the buffeting lift, even at the lowest Re tested, is closer to a Gaussian random signal than a periodic sine signal.

Sample plots of the probability density function (p.d.f.) of the buffeting lift and drag due to a turbulent cross flow created by a 50·8 mm grid at two different Re are shown in figure 20. Since the SAICOR Correlation and Probability Analyzer gives a probability density function for a Gaussian random noise in terms of $\sigma P(F_L)$ *vs.* F_L, where

$$P(F_L) = \frac{\sigma}{(2\pi)^{\frac{1}{2}}} \exp\left[-\frac{(F_L - m)^2}{2\sigma^2}\right],$$

m is the mean value of the event F_L and σ is the standard deviation, the output can be easily normalized when m and σ of the input signal are known. The load cells are set to resolve the a.c. component of the signals only, therefore, $m \equiv 0$ and σ^2 is the mean-square value of the unsteady forces. The p.d.f. shown in figure 20 is plotted with $P(z)$ versus z where $z = F_L^2/2\sigma^2$. For comparison purposes, the normalized p.d.f. of a Gaussian random signal where $\sigma = (2\pi)^{\frac{1}{2}}$ is also plotted. It can be seen that at the lowest Re tested, the lift signal is quasi-periodic while at high Re it is of the wide-band random type. This is consistent with the statistical analysis of the signal. On the other hand, the drag signal is of the wide-band random type even at low Re.

Finally, Roshko's (1961) postulate that changes in base pressure are closely related to changes in C_D is again tested for the buffeting case. The data used to test this postulate are selected from the fluctuating lift signals of the 114·3 mm active span cylinder. Results in the form of $C_D St$ *vs.* $k = [1-(C_p)_b]^{\frac{1}{2}}$ are plotted in figure 21, in which the measured data of Roshko (1961), Bearman (1967), and Surry (1972) are also shown for comparison. To determine St for the buffeting lift, the location of the peak in the auto-power spectrum is taken to give the dominant frequency. For those spectra where no peaks are discernible, the St cannot be calculated and therefore $C_D St$ *vs.* k results are not presented, It can be seen that all data points thus obtained lie on a single curve. Also, they are very well correlated by the semi-theoretical curve proposed by Bearman (1967). Therefore, the postulate that the wake dominates the response of the cylinder is also true for the buffeting case, at least for low Re where a dominant frequency for the buffeting lift signal can be identified.

5. Conclusions

From the results presented in § 4, the following conclusions can be drawn. These are:

(1) Effects of free-stream turbulence on both the steady mean drag and the unsteady lift and drag are to shift the transitional region to a lower Re range.

(2) At pre-transitional Re, free-stream turbulence has little or no effect on the steady and unsteady forces.

(3) There is a strong similarity between the variation of the steady drag with Re and of the unsteady lift and drag with Re. This is true for both uniform and turbulent cross flows over single cylinders.

(4) At the same Re, the mean drag coefficient can be used to obtain a conservative estimate of C_L'. The ratio of C_L'/C_D varies from 0·8 at pre-transitional Re to 0·2 at transitional Re.

(5) As Re is increased from 3×10^4 to 4×10^5, the character of the buffeting lift signal changes from quasi-periodic to wide-band random, the p.d.f. of which resembles that of a Gaussian.

(6) The measured C_L' is found to depend on cylinder span, with the result that shorter span gives higher C_L'. This can be explained by the fact that the forces are not perfectly correlated in the spanwise direction. The lack of perfect correlation may be attributable to the variation of the circumferential position of the boundary-layer separation on the cylinder surface.

(7) In the case of single cylinders in turbulent cross flows, the results also suggest that changes in C_D are closely related to changes in base pressure, an established fact in the case of uniform cross flows.

The authors are most grateful for the hospitality and co-operation extended to them by the Applied Research Laboratory, Pennsylvania State University, State College, Pennsylvania. In the absence of the first author (R.M.C.S.), the experiment was supervised by Professor G. Gurney of the Applied Research Laboratory. The experiments were also assisted by Mr Leon LaGalles of General Electric. Funding support by the Nuclear Energy Engineering Division, General Electric Company, through DoE Contract no. EN-77-C-02-4175 is acknowledged.

REFERENCES

ACHENBACH, E. 1968 Distribution of local pressure and skin friction around a circular cylinder in cross-flow up to $Re = 5 \times 10^6$. *J. Fluid Mech.* **34**, 625.

BATHAM, J. P. 1973 Pressure distributions on circular cylinders at critical Reynolds numbers. *J. Fluid Mech.* **57**, 209.

BEARMAN, P. W. 1967 On vortex street wakes. *J. Fluid Mech.* **28**, 625

BEARMAN, P. W. 1969 On vortex shedding from a circular cylinder in the critical Reynolds-number regime. *J. Fluid Mech.* **37**, 577.

BENDAT, J. S. & PIERSOL, A. G. 1971 *Random Data: Analysis and Measurement Procedures.* Wiley-Interscience.

BISHOP, R. E. D. & HASSAN, A. Y. 1964 The lift and drag forces on a circular cylinder in a flowing fluid. *Proc. Roy. Soc.* A **277**, 32.

BRUUN, H. H. & DAVIES, P. O. A. L. 1975 An experimental investigation of the unsteady pressure forces on a circular cylinder in a turbulent crossflow. *J. Sound & Vib.* **40**, 535.

DELANY, N. K. & SORENSEN, N. E. 1953 Flow speed drag of cylinders of various shapes. *N.A.C.A.* TN-3038.

FUNG, Y. C. 1960 Fluctuating lift and drag acting on a cylinder in a flow at supercritical Reynolds numbers. *J. Aero. Sci.* **27**, 801.

GERRARD, J. H. 1961 An experimental investigation of the oscillating lift and drag of a circular cylinder shedding turbulent vortices. *J. Fluid Mech.* **11**, 244.

GOLDSTEIN, S. 1965 *Modern Developments in Fluid Dynamics*, vol. II, p. 493. Dover.

HUMPHREYS, J. S. 1960 On a circular cylinder in a steady wind at transition Reynolds numbers. *J. Fluid Mech.* **9**, 603.

JONES, G. W., CINCOTTA, J. J. & WALKER, R. W. 1968 Aerodynamic forces on a stationary and oscillating circular cylinder at high Reynolds numbers. *N.A.S.A.* TR R-300.

LEE, B. E. 1975 Some effects of turbulence scaling on the mean forces on a bluff body. *J. Ind. Aerodynamics* **1**, 316.

LEHMAN, A. F. 1959 The Garfield Thomas Water Tunnel. *Pennsylvania State Univ. Rep.* no. NOrd 16597-57.

LOISEAU, H. & SZECHENYI, E. 1972 Analyse expérimentale des portances sur un cylindre immobile soumis à un écoulement perpendiculaire à son axe à des nombres de Reynolds élevés. *Recherche Aerospatiale* **5**, 279.

PETTY, D. G. 1979 The effects of turbulence intensity and scale on the flow past square prisms. *J. Ind. Aerodynamics* **4**, 247.

RAMAMURTHY, A. S. & BHASKARAN, P. 1977 Constrained flow past cavitating bluff bodies. *Trans. A.S.M.E.* I, *J. Fluids Engng* **99**, 717.

RELF, E. F. & SIMMONS, L. F. G. 1924 The frequency of the eddies generated by the motion of circular cylinders through a fluid. *Aero. Res. Counc. R. & M.* 917.

RICHTER, A. & STEFAN, K. 1973 Anwendung piezoelektrischer Mehrkompouenten-Kraftmesser in der Stromungsmechanik. *Arch. Tech. Messen* **5**, 131.

RICHTER, A. & NAUDASCHER E. 1976 Fluctuating forces on a rigid circular cylinder in confined flow. *J. Fluid Mech.* **78**, 561.

ROSHKO, A. 1961 Experiments on the flow past a circular cylinder at very high Reynolds number. *J. Fluid Mech.* **10**, 345.

SAVKAR, S. D. & SO, R. M. C. 1978 On the buffeting response of a cylinder in a turbulent crossflow. *TIS Rep.* no. 78 CRD 119. Research and Development Center, General Electric Company. Also published in *BNES Conf. - Vibration in Nuclear Plant, Keswick, U.K.*, Paper 2.1.

SCHMIDT, L. V. 1965 Measurements of fluctuating air loads on a circular cylinder. *J. Aircraft*, **2**, 49.

SCHMIDT, L. V. 1966 Fluctuating force measurements upon a circular cylinder at Reynolds numbers up to 5×10^6. *N.A.S.A.* TM X-57, 779, 15.1.

SCHMIDT, L. V. 1970 Influence of Spatial Correlation upon Load Resolution. *J. Spacecraft*, **7**, 363.

SO, R. M. C. 1979 An experimental investigation of circular cylinders in crossflows. *Nuclear Energy Engng Div., G. E. C., San Jose, California, Report* no. GEAP-24176.

SURRY, D. 1972 Some effects of intense turbulence on the aerodynamics of a circular cylinder at subcritical Reynolds number. *J. Fluid Mech.* **52**, 543.

VICKERY, B. J. 1966 Fluctuating lift and drag on a long cylinder of square cross section in a smooth and in a turbulent stream. *J. Fluid Mech.* **25**, 481.

WIESELSBERGER, G. 1923 Der Widerstand von Zylinden, Ergebnisse der Aerodynamischen Versuchsanstalt Göttingen, II. *Lieferung*, p. 23.